Heliyon 10 (2024) e25185

Contents lists available at ScienceDirect

Heliyon

journal homepage: www.cell.com/heliyon

Research article

Contrast-enhanced ultrasound (CEUS) and shear wave elastography (SWE) features for characterizing serous microcystic adenomas (SMAs): In comparison to pancreatic neuroendocrine tumors (pNETs)

Xiao-Fan Tian [a,1], Ling-Yun Yu [b,1], Dao-Hui Yang [b], Dan Zuo [c], Jia-Ying Cao [a], Ying Wang [a], Zi-Yi Yang [e], Wen-Hui Lou [d], Wen-Ping Wang [c], Wei Gong [e], Yi Dong [a,*]

[a] *Department of Ultrasound, Xinhua Hospital Affiliated to Shanghai Jiaotong University School of Medicine, 200092, Shanghai, China*
[b] *Department of Ultrasound, Xiamen Branch, Zhongshan Hospital, Fudan University, 361006, Xiamen, China*
[c] *Department of Ultrasound, Zhongshan Hospital, Fudan University, 200032, Shanghai, China*
[d] *Department of Pancreatic Surgery, Zhongshan Hospital, Fudan University, 200032, Shanghai, China*
[e] *Department of Surgery, Xinhua Hospital Affiliated to Shanghai Jiaotong University School of Medicine, 1665 Kongjiang Road, Shanghai, 200092, China*

ARTICLE INFO

Keywords:
Serous microcystic adenomas (SMAs)
Pancreatic neuroendocrine tumors (pNETs)
Contrast-enhanced ultrasound (CEUS)
Shear wave elastography (SWE)
Virtual touch tissue imaging and quantification (VTIQ)

ABSTRACT

Objectives: Serous microcystic adenoma (SMA), a primary benign pancreatic tumor which can be clinically followed-up instead of undergoing surgery, are sometimes mis-distinguished as pancreatic neuroendocrine tumor (pNET) in regular preoperative imaging examinations. This study aimed to analyze preoperative contrast-enhanced ultrasound (CEUS) and shear wave elastography (SWE) features of SMAs in comparison to pNETs.

Material and methods: In this retrospective study, patients with imaging-diagnosed pancreatic lesions were screened between October 2020 to October 2022 (ethical approval No. B2020-309R). Performing by a Siemens Sequoia (Siemens Medical Solutions, Mountain View, CA, USA) equipped with a 5C-1 curved array transducer (3.0–4.5 MHz), CEUS examination was conducted to observe the microvascular perfusion patterns of pancreatic lesions in arterial phase, venous/late phases (VLP) using SonoVue® (Bracco Imaging Spa, Milan, Italy) as the contrast agent. Virtual touch tissue imaging and quantification (VTIQ) – SWE was used to measure the shear wave velocity (SWV, m/s) value to represent the quantitative stiffness of pancreatic lesions.

Abbreviations: **ADC**, apparent diffusion coefficient; **AUROC**, area under the receiver operating characteristic curve; **BMI**, body mass index; **BMUS**, B-mode ultrasound; **CA-125**, cancer antigen-125; **CA-199**, cancer antigen-199; **CDFI**, Color Doppler flow imaging; **CEA**, serum carcinoembryonic antigen; **CEUS**, contrast-enhanced ultrasound; **CT**, computed tomography; **DWI**, diffusion-weighted imaging; **EFSUMB**, European Federation of Societies for Ultrasound in Medicine and Biology; **EUS**, endoscopic ultrasound; **MI**, mechanical index; **MPD**, main pancreatic duct; **MRI**, magnetic resonance imaging; **NES**, neuron-specific enolase; **NPV**, negative predictive value; **PET/CT**, positron emission tomography/computed tomography; **pNEC**, pancreatic neuroendocrine carcinoma; **pNET**, pancreatic neuroendocrine tumor; **PPV**, positive predictive value; **ROI**, regions of interests; **RI**, resistive index; **SMA**, Serous microcystic adenoma; **SR**, strain ratio; **SWE**, shear wave elastography; **SWV**, shear wave velocity; **VLP**, venous/late phases; **VTIQ**, Virtual touch tissue imaging and quantification.

* Corresponding author. Department of Ultrasound, Xinhua Hospital Affiliated to Shanghai Jiaotong University School of Medicine, 1665 Kongjiang Road, Shanghai, 200092, China.
E-mail address: drdaisydong@hotmail.com (Y. Dong).
[1] share the co-first authorship.

https://doi.org/10.1016/j.heliyon.2024.e25185
Received 12 October 2023; Received in revised form 19 January 2024; Accepted 22 January 2024

Multivariate logistic regression was performed to analyze potential ultrasound and clinical features in discriminating SMAs and pNETs.
Results: Finally, 30 SMA and 40 pNET patients were included. All pancreatic lesions were pathologically proven via biopsy or surgery. During the arterial phase of CEUS, most SMAs and pNETs showed iso- or hyperenhancement (29/30, 97 % and 31/40, 78 %), with a specific early honeycomb enhancement pattern appeared in 14/30 (47 %) SMA lesions. During the VLP, while most of the SMA lesions remained iso- or hyperenhancement (25/30, 83 %), nearly half of the pNET lesions revealed an attenuated hypoenhancement (17/40, 43 %). The proportion of hypoenhancement pattern during the VLP of CEUS differed significantly between SMAs and pNETs ($P = 0.021$). The measured SWV value of SMAs was significantly higher than pNETs (2.04 ± 0.70 m/s versus 1.42 ± 0.44 m/s, $P = 0.002$). Taking a SWV value > 1.83 m/s as a cutoff in differentiating SMAs and pNETs, the area under the receiver operating characteristic curve (AUROC) was 0.825, with sensitivity, specificity and likelihood ratio (+) of 85.71 %, 72.73 % and 3.143, respectively. Multivariate logistic regression revealed that SWV value (m/s) of the pancreatic lesion was an independent variable in discriminating SMA and pNET.
Conclusion: By comprehensively evaluating CEUS patterns and SWE features, SMA and pNET may be well differentiated before the operation. While SMA typically presents as harder lesion in VTIQ-SWE, exhibiting a specific honeycomb hyperenhancement pattern during the arterial phase of CEUS, pNET is characterized by relative softness, occasionally displaying a wash-out pattern during the VLP of CEUS.

1. Introduction

Pancreatic cystic lesions have a reported prevalence between 3.1 and 12.6 % [1]. Serous cystadenomas, as common primary cystic pancreatic neoplasms, can be morphologically classified as microcystic, oligocystic, solid and mixed patterns [2–4]. Among these, serous microcystic adenoma (SMA) is the most common subtype, account for approximately 45 %–70 % [4]. Unlike other pancreatic lesions that surgical treatment is considered to be the primary therapeutic choice, SMA can be clinical followed-up without active intervention due to its relatively low malignant potential [5,6].

Since most of the patients with SMA have no obvious clinical signs or symptoms, they are usually discovered by routine imaging screening such as ultrasound or computed tomography (CT) [7,8]. According to the previous reports, while the specific enhancement pattern of SMA appears only during the very early stage of the arterial phase, it's usually difficult to be captured after the injection of contrast agent during the contrast enhanced CT (CECT) assessment, which may lead to misdiagnosis [9,10]. A precise imaging diagnosis with more widespread accessibility is important for clinical decision-making process, which may help avoiding inappropriate medical treatments, and improve the prognosis of patients [2,6].

Conventional B-mode ultrasound (BMUS), as a convenient, radiation-free imaging method, is commonly used in screening potential pancreatic lesions [11,12]. With the combination of contrast-enhanced ultrasound (CEUS), the real-time microvascular perfusion patterns may be observed and evaluated, which can help discriminating pancreatic lesions [8,13]. However, due to the rarity of the disease, there is limited data on the CEUS imaging features of SMA [8]. Pancreatic neuroendocrine tumor (pNET), as another rare pancreatic neoplasm that usually be misdiagnosed as SMA, can show malignant potential with infiltrated growth pattern [14,15]. As a result, surgical treatment would be recommended to be the primary therapeutic choice, especially for Grade 3 (G3) pNET or pNEC (pancreatic neuroendocrine carcinoma) (2017 WHO classification) [16]. Since the combination of BMUS/CEUS can provide further clues in differential diagnosis of SMA and pNET, it may be helpful in guiding therapeutic choice [17,18]. Furthermore, while rare research has paid attention to the venous/late phase (VLP) of pancreatic CEUS examination, the wash-out pattern during VLP may also reflect the malignant tendency of pancreatic tumors [8,11,18,19].

On the other hand, ultrasound shear wave elastography (SWE), as an imaging method that can make a precise and quantitative evaluation of pancreatic stiffness, few studies have investigated its potential usefulness in differential diagnosis of pancreatic lesions [20–23]. Previous report suggested that pathological pancreatic lesions were usually harder than normal pancreatic parenchyma because of the desmoplasia with fibroblasts proliferation [24]. While the quantitative shear wave velocity (SWV) is considered be correlated with the fibrosis degree of pancreatic tissue, the application of SWE may also improve preoperative diagnosis [25].

The aim of this study is to illustrate CEUS and SWE features of pathologically proven SMA, in comparison to pNET. And investigate the potential usefulness of multi-modality ultrasound in differential diagnosis of benign/borderline pancreatic tumors, which may help in patient management and avoid excessive therapeutic choices.

2. Materials and methods

2.1. Institutional board approval

This single-centered study was approved by the institutional review board of our institution (Approval No. B2020-309R). Informed consent was signed, and all the procedure was followed in accordance with the Declaration of Helsinki. All the participants consented to have their medical images published.

2.2. Patients

This study initially screened patients with imaging diagnosed (US, CT, magnetic resonance imaging (MRI), positron emission tomography/computed tomography (PET/CT)) pancreatic lesions and admitted to our hospital between October 2020 to October 2022. The inclusion criteria were [1]: Patients aged above 18 years old [2]; Pancreatic lesions can be clearly visualized on BMUS scan, with detectable solid structure [3]; No history of contrast agent allergy or other specific foods or drugs allergy. All the patients received CEUS and VTIQ-SWE assessment within one week before the surgery (pancreatectomy or laparotomy exploration) or biopsy. The exclusion criteria were [1]: Whole cystic degeneration of lesion which make SWE assessment unable to be performed [2]; Patients lack of final histopathological diagnosis [3]; Patients who were unable to cooperate in CEUS, SWE or other necessary assessments [4]; Over-weighted patients with body mass index (BMI) $\geq$ 28, which makes SWE assessment hard to conduct.

2.3. Study protocol

Firstly, patient's clinical data were recorded, including gender, age and associated laboratory test results (serum carcinoembryonic antigen (CEA), cancer antigen-199 (CA-199), cancer antigen-125 (CA-125), neuron-specific enolase (NSE) and amylase level).

BMUS and CEUS examinations were performed by three experienced radiologists with more than 5 years of pancreatic CEUS experience, who were also aware of the patients' clinical histories. All ultrasound examinations were performed using a Siemens ACUSON Sequoia (Siemens Medical Solutions, Mountain View, CA, USA) with a 5C-1 curved array transducer (3.0–4.5 MHz) equipped. SWE assessment was conducted with the build-in virtual touch tissue imaging and quantification (VTIQ) feature.

Histopathological assessment, on the basis of hematoxylin-eosin-stained sections and immunohistochemical staining results, was performed to defined the final diagnosis of lesions. pNETs were graded into G1 (Ki-67 index $\leq$2 %), G2 (Ki-67 index = 3–20 %) or G3/pNEC (Ki-67 index >20 %) according to the 2017 WHO classification standard.

2.4. B mode ultrasound (BMUS)

The BMUS manifestations including size (mm), margin (ill- or well-defined appearance), echogenicity (hypo-, iso- or hyperechogenic), homogeneity (homo- or heterogeneous) and the existence of cystic degeneration or calcification of pancreatic lesions were firstly defined and recorded. Main pancreatic duct (MPD) was observed and a dilated MPD ($\geq$3 mm) would be recorded. Color Doppler flow imaging (CDFI) was used to detect the blood flow signals of the lesions.

2.5. Contrast-enhanced ultrasound (CEUS)

CEUS was performed using SonoVue® (Bracco Imaging Spa, Milan, Italy) as the contrast agent at a low mechanical index (MI) of 0.05–0.30. Patients were instructed to fast for at least 8 h prior to the procedure. A 1.5 ml bolus of contrast agent was then injected i.v. followed by a 5 ml bolus of saline solution. A real-time and dynamic observation of contrast-enhanced phases began instantly after the injection. According to the current European Federation of Societies for Ultrasound in Medicine and Biology (EFSUMB) guidelines of CEUS in pancreatic examination, the CEUS phases were divided into arterial (0–30 s), venous (30–120 s) and late phases (120–300 s) [26]. Repeated injection of contrast agent was permitted when necessary. The enhancement of the lesion compared to the surrounding pancreatic parenchyma (hypo-, iso- or hyperenhancement), the homogeneity of enhancement (homo- or heterogeneous) and additional features, such as necrosis, calcification or specific enhancement configurations were observed. All examinations were digitally recorded in DICOM format for further analysis.

2.6. Virtual touch tissue imaging and quantification (VTIQ)

On SWE assessment, the applying of VTIQ could first visualize the relative elasticity of pancreas with a square sampling frame, which allowed us to evaluate the measurement quality and select appropriate regions of interests (ROIs) for quantifying the stiffness of target tissue. The patients were instructed to hold their breath for several seconds, and some pressure would be applied during the assessment to shorten the distance between the probe and the pancreatic tissue to ensure optimal measurement depth (2–10 cm) [27]. Afterwards, avoiding the dilated MPD or any other interferences (gastrointestinal gas, surrounding vascular structure, etc.), three equal-sized ROIs were set in the same depth of lesion to measure the SWV (m/s) value. The procedure was repeated three times and calculated the mean SWV value to represent quantitative stiffness of pancreatic lesions.

2.7. Statistics analysis

Statistical analyses were performed with SPSS statistics 26.0 (SPSS Inc., Chicago, IL, United States) in this study. Applying Shapiro-Wilk test to assess the normality of variables, continuous data were presented as either mean $\pm$ standard deviation or median with range depended on its distribution. Descriptive data were described in number with percentage. Student's T-test, for the normally distributed continuous variables; $\chi 2$ test, for the normally distributed discrete variables; and Mann-Whiney *U* test, for skewed distributed variables or under the condition of unequal variance between the two independent sampling groups, were used to compare the variables between SMAs and pNETs. For the features that played potentially significant roles in differential diagnosis, multivariate logistic regression analysis was performed to control the confounding. Since we enrolled pathologically proven SMA and pNET only,

we may define either of them as dependent variable. In this study, pNET is defined as positive result while it's more likely to show malignant tendency. The receiver operating characteristic (ROC) analysis was conducted to define the cutoff SWV value (m/s) for differentiating SMA and pNET, and evaluate the diagnostic efficacy of VTIQ-SWE assessment.

3. Results

3.1. Overall characteristics

According to the inclusion and exclusion criteria, among the 462 scanned patients, 30/462 pathologically proven SMAs (6.5 %) and 40/462 pNETs (8.7 %) were identified in 23/70 males (32.9 %) and 47/70 females (67.1 %) aged between 55.2 ± 11.7 years (range 28–76 years, median 54 years) (Fig. 1-g, 1-h, 1-i; 2-h, 2-i). According to 2017 WHO classification, 9 (9/40, 22.5 %), 18 (18/40, 45 %) and 13 (13/40, 32.5 %) pNETs were pathologically grading as G1, G2 and G3/pNEC, respectively. General characteristics of patients were shown in Table 1. The proportion of female ($P = 0.003$) and the average age of patients ($P = 0.042$) were statistically higher in the SMA group compared to the pNET group. Serum CEA, CA125, CA199, NSE and amylase level did not differ significantly between the two groups ($P > 0.05$).

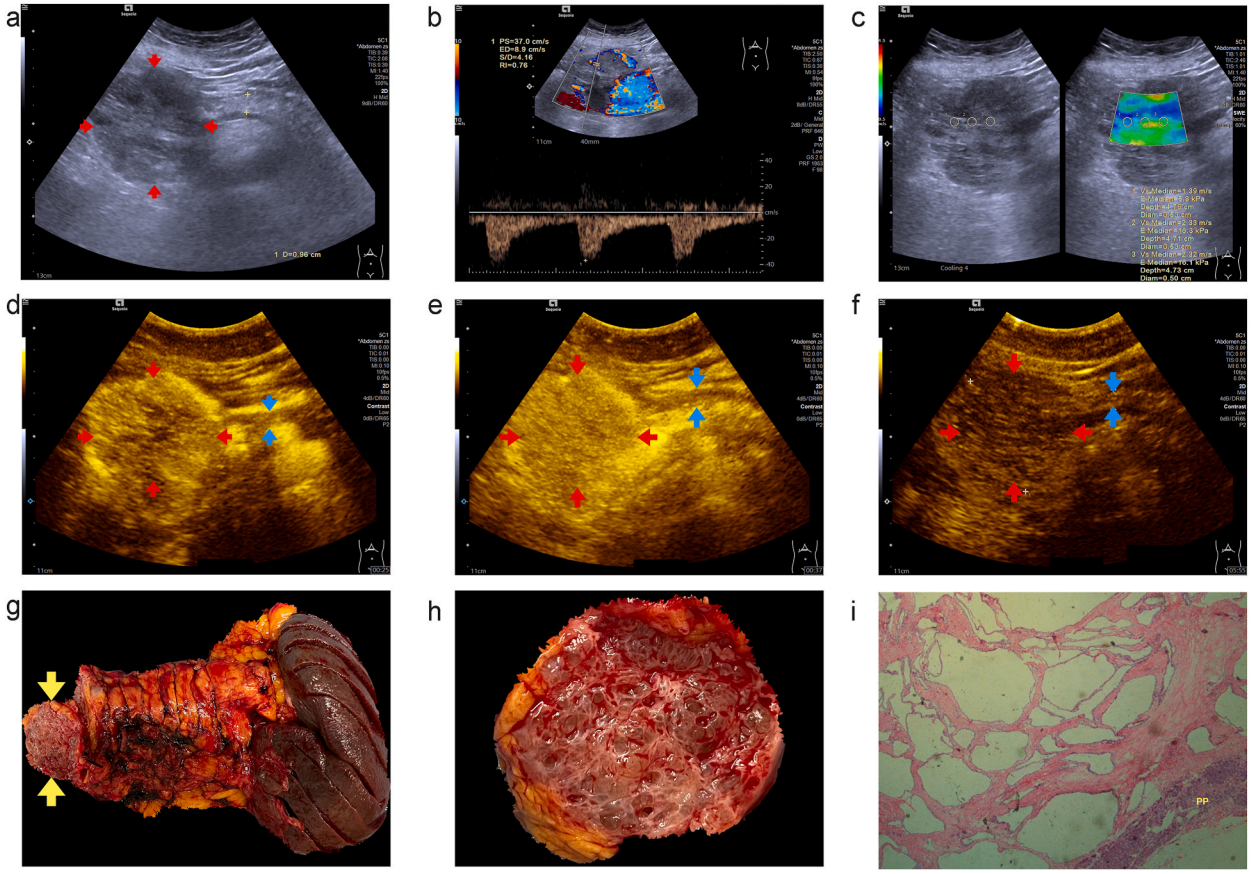

Fig. 1. A case of serous microcystic adenoma (SMA). B-mode ultrasound image showed a large, heterogenous and well-defined hypoechogenic focal pancreatic lesion with indistinct cystic structure, located in head-body part of pancreas (red arrows). The adjacent pancreatic parenchyma was observed in the superficial layer of splenic vein (yellow crosses) (a). Cyclic perilesional and short-linear intralesional vessels were detected in color Doppler flow imaging (CDFI), with resistive index (RI) of 0.76 (b). The lesion presented mixed green and blue color in virtual touch tissue imaging and quantification (VTIQ) image, with quantitative shear wave velocity (SWV) value ranged between 1.39 and 2.33 m/s (c). The lesion showed hyperenhancement during the arterial phase (red arrows) compared to the surrounding parenchyma (blue arrows). A honeycomb pattern was observed (d). During venous phase, the lesion remained hyperenhancement (e). The lesion appeared isoenhancement during the late phase (f). Gross pathology photograph showed a well-marginated, multiloculated mass, with a collection of microcysts that ranged between several millimeters in size (g–h). Histopathologic slide presented a large number of small cysts with single-layered cuboidal cells wall. A clear margin was shown between the lesion and the surrounding pancreatic parenchyma (PP) (i). (For interpretation of the references to color in this figure legend, the reader is referred to the Web version of this article.)

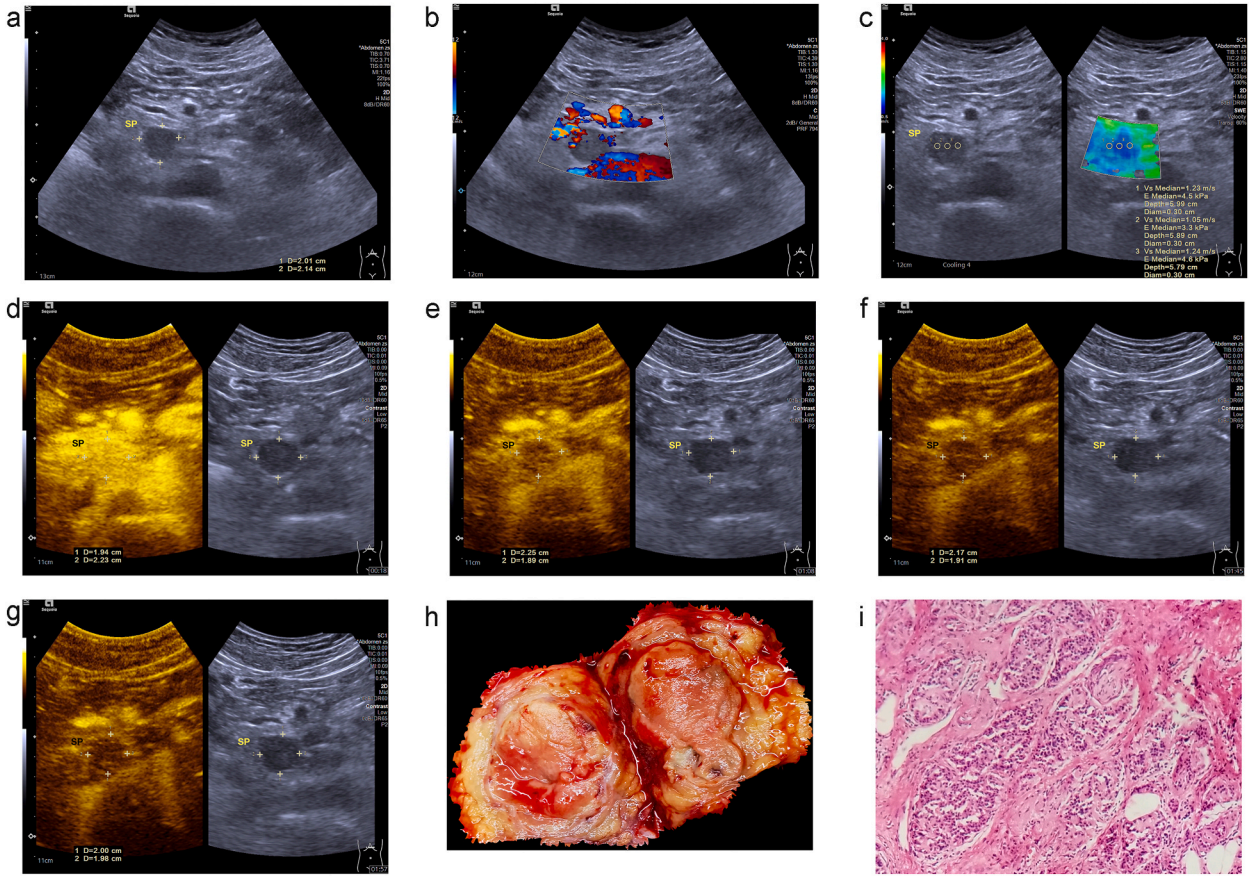

Fig. 2. A case of a Grade 3 (G3) pancreatic neuroendocrine tumor (pNET). B-mode ultrasound image showed a solid, homogenous and well-defined hypoechogenic focal pancreatic lesion located in the head-neck part of pancreas (yellow crosses), surrounding parenchyma (SP) was shown (a). Intralesional punctiform color flow signals were detected (b). The lesion presented uneven blue color in virtual touch tissue imaging and quantification (VTIQ) image, with quantitative shear wave velocity (SWV) value ranged between 1.05 and 1.24 m/s (c). The lesion showed hyperenhancement during the arterial phase compared to SP (d). The lesion showed progressive washout during the venous/late phase (VLP) compared to SP (e–g). Gross pathology photograph showed solid component with intralesional hemorrhage (h). The histopathological slide presented a homogenous appearance of pNET, with high cellularity and poor fibrotic stroma (i). (For interpretation of the references to color in this figure legend, the reader is referred to the Web version of this article.)

Table 1
General characteristics of patients.

	SMAs (n = 30)	pNETs (n = 40)	P-value
Baseline characteristics			
Gender (n, %)			
Male	4 (13 %)	19 (47.5 %)	**0.003***
Female	26 (87 %)	21 (52.5 %)	
Age (years)			
Mean ± SD	58.47 ± 11.38	52.78 ± 11.40	**0.042***
Range	33–76	28–76	
Histopathological result (n, %)			
Pancreatectomy	22 (73 %)	34 (85 %)	0.277
EUS-FNA/exploratory laparotomy	8 (27 %)	6 (15 %)	
Laboratory tests			
CEA (ref. <5 ng/ml)	1.588 ± 0.763	1.729 ± 0.772	0.479
CA125 (ref. 0–24 U/ml)	12.612 ± 8.469	10.018 ± 4.858	0.174
CA199 (ref. <34 U/ml)	9.928 ± 5.429	8.437 ± 5.853	0.313
NSE (ref. <16.3 ng/ml)	12.775 ± 2.236	13.885 ± 2.223	0.125
Serum amylase level (ref. <220 U/L)	69.800 ± 38.226	73.686 ± 60.154	0.796

CA125: cancer antigen 125; CA199: cancer antigen 199; CEA: carcinoembryonic antigen; EUS-FNA: endoscopic ultrasound fine-needle aspiration; NSE: neuron-specific enolase; pNETs: pancreatic neuroendocrine tumors; SD: standard deviation; SMAs: serous microcystic adenomas; *: P < 0.05

3.2. BMUS features

On conventional BMUS, both SMA and pNET mainly manifested as solid-like, well-defined hypoechogenic lesion ($P > 0.05$) (Fig. 1-a; 2-a). Anechogenic necrotic or hemorrhagic areas inside the lesions was more commonly detected in pNETs. The proportion of dilated MPD (≥3 mm) detected was in no difference between SMAs and pNETs ($P = 0.122$). Color blood signals could be detected in both SMAs (10/30, 33 %) and pNETs (7/40, 17.5 %), and the measured resistive index (RI) did not differ significantly between the two lesions ($P = 0.226$) (Fig. 1-b; 2-b). The lesion size was larger within the SMA patients compared to the pNET patients ($P < 0.001$) (Table 2).

3.3. CEUS pattern

On CEUS, most SMA and pNET lesions presented iso- or hyperenhancement (29/30, 97 %; 31/40, 78 %) during the arterial phase (Fig. 1-d; 2-d). A honeycomb enhancement pattern appeared in 14/30 (47 %) SMAs during the very early stage of arterial phase, which did not appear in pNETs ($P < 0.001$) (Table 2). Both two types of pancreatic tumors usually showed a rapid and intense enhancement, and necrotic areas can sometimes be observed in larger lesions. During VLP, while SMAs mostly remained iso- or hyperenhancement (25/30, 83 %), pNETs could sometimes show attenuated enhancement compared to the surrounding pancreatic parenchyma (17/40, 43 %) (Figs. 1-e, f, 2-e, f, g). The proportion of lesions with progressive washout pattern during the VLP was statistically higher in pNET compared to SMA ($P = 0.021$) (Table 2).

3.4. VTIQ-SWE measurements

VTIQ images illustrated the relative elasticity of pancreatic lesions (blue, soft; green, medium; red, hard). While SMA usually appeared as a mixed green and blue mass, pNET usually showed uneven blue color, which suggested that SMA may be relatively harder (Fig. 1-c; 2-c).

The mean SWV value (m/s) of SMAs (2.04 ± 0.70 m/s, range 1.23–3.82 m/s, median 1.93 m/s), which represent the quantitative stiffness of lesion, was significantly higher than pNETs (1.42 ± 0.44 m/s, range 0.84–2.63 m/s, median 1.38 m/s) ($P = 0.002$) (Table 2).

The ROC curve analysis was performed to evaluate the diagnostic efficacy of SWE in differential diagnosis of SMA and pNET. A cutoff SWV value of 1.83 m/s was obtained through maximizing Youden index [28]. SMA is more likely to be diagnosed while the measured SWV value (m/s) of lesion is higher than 1.83 m/s. The area under the ROC curve was 0.825, with sensitivity, specificity, positive predictive value (PPV), negative predictive value (NPV) and likelihood ratio (+) of 85.71 %, 72.73 %, 75.86 %, 83.58 % and

Table 2
BMUS, CEUS and SWE features of SMAs and pNETs.

	SMAs ($n = 30$)	pNETs ($n = 40$)	*P*-value
BMUS features			
Size (mm)	40.9 ± 21.7	23.7 ± 11.2	**<0.001***
Echogenicity (*n*, %)			
Hypoechogenic	25 (83 %)	38 (95 %)	0.107
Iso/hyperechogenic	5 (17 %)	2 (5 %)	
Homogeneity (*n*, %)			
Homogenous	18 (60 %)	22 (55 %)	0.676
Heterogenous	12 (40 %)	18 (45 %)	
Margin (*n*, %)			
Well-defined	25 (83 %)	28 (70 %)	0.198
Ill-defined	5 (17 %)	12 (30 %)	
CDFI (*n*, %)			
Intra/peri-lesional vessels	10 (33 %)	7 (17.5 %)	0.126
RI	0.57 ± 0.07	0.64 ± 0.13	0.226
Dilated MPD (≥3 mm)	6 (20 %)	3 (7.5 %)	0.122
CEUS features			
Arterial phase (*n*, %)			
Hypoenhancement	1 (3 %)	9 (22.5 %)	0.065
Isoenhancement	16 (53 %)	9 (22.5 %)	
Hyperenhancement	13 (43 %)	22 (55 %)	
Honeycomb enhancement pattern	14 (47 %)	0 (0 %)	**<0.001***
Venous/late phase (*n*, %)			
Hypoenhancement	5 (17 %)	17 (42.5 %)	**0.021***
Isoenhancement	22 (73 %)	17 (42.5 %)	
Hyperenhancement	3 (10 %)	6 (15 %)	
SWE feature			
Lesion SWV value (m/s)	2.04 ± 0.70	1.42 ± 0.44	**0.002***

BMUS: B mode ultrasound; CDFI: color Doppler flow imaging; CEUS: contrast enhanced ultrasound; MPD: main pancreatic duct; pNETs: pancreatic neuroendocrine tumors; RI: resistive index; SMAs: serous microcystic adenomas; SWE: shear wave elastography; SWE: shear wave elastography; SWV: shear wave velocity; *: $P < 0.05$.

3.143, respectively (Fig. 3).

3.5. Ultrasound and clinical features in discriminating SMA and pNET

Multivariate logistic regression analysis was conducted to evaluate the diagnostic efficacy of potential ultrasound and clinical features in differential diagnosis of SMA and pNET, and control the confounding. Variables including patients' general characteristics (gender (male/female) and age (years)), BMUS specifics (size (mm) and CDFI blood flow), CEUS features (existence of early arterial phase honeycomb enhancement pattern and VLP hypoenhancement pattern) and SWV value (m/s) of pancreatic lesions were analyzed. The SWV value (m/s) of lesion (OR = 0.043, 95 %CI [0.017, 0.602], $P = 0.012$) was identified as an independent variable that differed significantly between SMA and pNET (Table 3).

4. Discussion

For primary pancreatic malignancies, regular enhanced imaging methods can usually provide adequate diagnostic efficacy due to the typical hypovascular appearance of lesions [29]. However, for the wide variety of benign or borderline pancreatic tumors, a wide spectrum of imaging appearance sometimes makes the preoperative differential diagnosis difficult, which may cause inappropriate clinical management for patients [4,9,12,18,30].

SMA, as primary benign pancreatic tumor that does not usually require surgical treatment, its general hypervascular configuration during the arterial phase of CECT scan usually mimics other benign or borderline pancreatic tumors [1,4,9,10]. In this study, we used CEUS as a non-invasive imaging method to achieve a real-time observation of early arterial phase enhancement pattern of lesions and also the wash-out feature during VLP, and applied VTIQ-SWE in quantifying lesion stiffness for discriminating SMA and pNET.

Like SMA, pNET can also appear as high density and hypervascular configuration on CECT but with aggressive features [12,30]. On BMUS, since the microcystic structure of SMA is sometimes difficult to be clearly displayed, they can appear quite similar, both lesions show a hypoechogenic solid appearance with occasional larger cystic degeneration [12,18,30]. The lesion size of SMAs was considered to be larger when it's discovered compared to pNETs, which may attribute to the lack of obvious clinical manifestations. While the clinical signs/symptoms of SMA patients are usually caused by the oppression of larger occupancy to the surrounding tissue, some pNETs with endocrine function can generate extra amounts of hormones, such as gastrin, insulin and glucagon, which can cause specific clinical manifestations even when the lesion is smaller [18]. A dilated MPD (≥3 mm) was seldom detected in either SMA or pNET patients, and also there was no significant difference regarding CDFI blood flow patterns between the two tumors [18,19,31]. On CEUS, via a real-time observation right after the injection of contrast agent, a honeycomb enhancement pattern was detected only in SMAs [4,12]. Though it cannot always be observed in SMAs, especially when the lesion size was smaller, it's still suggested to be a very specific features that might be helpful in differentiating SMA from pNET [8,13]. During the VLP of CEUS, since SMA usually remained iso- or hyperenhancement, pNET could sometimes show hypoenhancement compared to the surrounding parenchyma. In our study, All the 13/13 (100 %) G3/pNEC lesions and 4/18 (22 %) G2 pNET lesions revealed a hypoenhancement pattern during VLP. pNETs with wash-out configuration may be associated with a poor differentiation, a higher pathological grade and a greater malignant

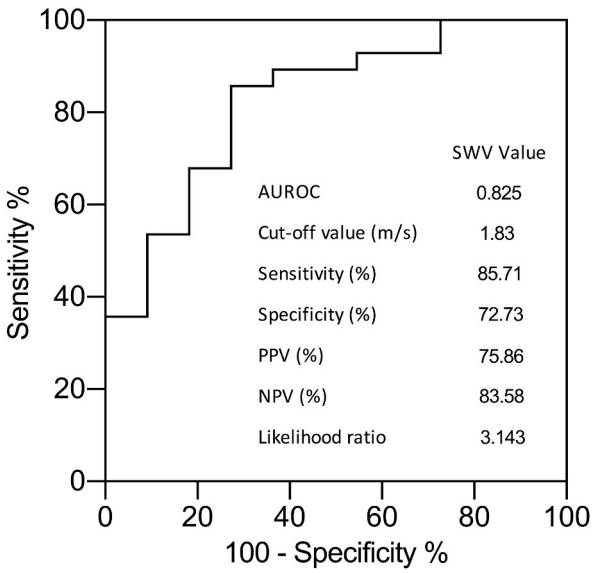

Fig. 3. Taking shear wave velocity (SWV) value of 1.83 m/s as a cutoff in differentiating SMAs and pNET, area under the receiver operating characteristic curve (AUROC) was 0.825 with 85.71 % sensitivity, 72.73 % specificity, 75.86 % positive predictive value (PPV) and 83.58 % negative predictive value (NPV), respectively.

Table 3
Multivariate logistic regression analysis of potential ultrasound and clinical features in differential diagnosis of SMA and pNET.

Variables	Univariate				Multivariate			
	OR	95 % CI		*P*-value	OR	95 % CI		*P*-value
		[0.025	0.975]			[0.025	0.975]	
Gender (male/female)	0.170	0.050	0.577	**0.004***				
Age (years)	0.956	0.915	0.999	**0.047***				
Size of lesion (mm)	0.939	0.905	0.975	**0.001***				
CDFI detected intra-/perilesional vessel (*n*)	2.357	0.774	7.182	0.131				
Honeycomb enhancement pattern (*n*)	4.04e+9	/	/	0.998				
VLP hypoenhancement (*n*)	0.271	0.086	0.852	**0.025***				
SWV (pancreatic lesion) (m/s)	0.082	0.021	0.323	**<0.001***	0.043	0.017	0.602	**0.012***
Constant								

CDFI: color Doppler flow imaging; CI: confidence interval; OR: odds ratio; pNET: pancreatic neuroendocrine tumor; SMA: serous microcystic adenoma; SWV: shear wave velocity; VLP: venous/late phase; *: $P < 0.05$.

potential [22]. Jeon et al. suggest that the hypovascular pNETs are closely related to the amount of dense and hyalinized stroma within the tumor and the distribution of intralesional vessels [32]. The proportion of hypoenhancement pattern was significantly higher in pNETs than in SMAs during the VLP, which could be considered as a CEUS feature in discriminating each other. On the other hand, MR - diffusion-weighted imaging (DWI) was reported to be useful in detecting pNETs, especially for localizing non-hypervascular ones, and in predicting pNETs grades by evaluating apparent diffusion coefficient (ADC) maps [33]. However, MRI also has disadvantages such as being expensive and having relatively complicated imaging processes.

While ultrasound elastography has been widely applied in differential diagnosis of liver diseases, previous studies have also shown preliminary promising results using SWE in estimating the stiffness of pancreatic lesions [21,22,34]. Havre et al. applied strain elastography under endoscopic ultrasound (EUS) in comparing strain ratio (SR) between pancreatic malignant and benign lesions [20]. They suggested that malignant pNET had higher SR than benign or indeterminate pNET, and SMA had even higher SR compared to pNET. However, EUS is a relatively invasive procedure and it's limited by the location and size of lesions, and the strain elastography is a qualitative evaluation method, the overall characteristic of pancreatic masses is sometimes hard to be fully observed and the measurement quality is difficult to be evaluated and controlled [21,22]. The application of *trans*-abdominal VTIQ-SWE allowed us to choose appropriate ROI to quantitatively evaluate the stiffness of target tissue, which may provide adequate reliability and repeatability. Our results suggested that the overall stiffness of SMA is greater than pNET, which may provide further information in differentiating the two pancreatic masses. The cutoff SWV value was calculated as 1.83 m/s via ROC analysis. The AUROC was 0.825, which showed relatively satisfactory diagnostic efficacy. The result of multivariate logistic regression analysis revealed that the SWV value (m/s) of lesion was independent variable that differed significantly between SMA and pNET.

There are some limitations of this study. First, conducting *trans*-abdominal ultrasound examinations of pancreas relies greatly on the experience of the operator. Since this is a retrospective study with relatively small sample size that collected by different practicians, the inter-observer's error should exist. Based on the findings of this preliminary study, we plan to conduct further investigation within geometrically different prospective cohorts to expand the sample size and control the confounding. Second, while a 2–10 cm measurement depth is a recommendation for elastography assessment to optimize the measurement quality, this method may not suitable for every patients (due to bowel gas or obesity, etc.) [27]. However, since VTIQ-SWE allows us to monitor the imaging quality while performing the SWV measurement, it may be easily handled by practicians with a short-term training. By Strictly follow the operating regulations, the measurement quality may be ensured, and may still provide adequate reliability and repeatability.

In conclusion, with the combination of BMUS-CEUS-SWE imaging modality, SMA and pNET may be well differentiated in a widespread available and low-cost access, which may help in therapeutic management and benefit to patients. Based on the findings of this study, we plan to expand the research subjects to other benign/borderline pancreatic tumors to further explore the usefulness and efficacy of multi-modality ultrasound imaging method in differential diagnosis.

5. Data availability statement

The authors confirm that the data supporting the findings of this study are available within the article. Raw data used to support the findings of this study will be made available from the corresponding author, upon reasonable request.

Ethics declarations

This study was reviewed and approved by the institutional review board of our institution, with the approval number: B2020-309R.

All participants/patients (or their proxies/legal guardians) provided informed consent for the publication of their anonymised case details and images.

Grand support

Supported by National Natural Science Foundation of China (No. 82071942, 82272013).
Supported by The Sino-German Mobility Programme of NSFC and DFG (Grant No. M-0504).
Sponsored by Shanghai Pujiang Program (No. 2020PJD008).

CRediT authorship contribution statement

Xiao-Fan Tian: Writing – review & editing, Writing – original draft, Methodology, Investigation, Formal analysis, Data curation, Conceptualization. **Ling-Yun Yu:** Writing – review & editing, Investigation, Data curation, Formal analysis. **Dao-Hui Yang:** Validation, Investigation, Data curation. **Dan Zuo:** Validation, Methodology, Investigation, Formal analysis. **Jia-Ying Cao:** Validation, Investigation, Data curation. **Ying Wang:** Validation, Investigation, Formal analysis. **Zi-Yi Yang:** Validation, Methodology, Data curation. **Wen-Hui Lou:** Writing – review & editing, Methodology, Investigation, Data curation, Conceptualization. **Wen-Ping Wang:** Writing – review & editing, Methodology, Investigation, Formal analysis. **Wei Gong:** Writing – review & editing, Validation, Methodology, Formal analysis, Data curation. **Yi Dong:** Writing – review & editing, Validation, Resources, Funding acquisition, Conceptualization.

Declaration of competing interest

The authors declare that they have no known competing financial interests or personal relationships that could have appeared to influence the work reported in this paper.

References

[1] G. Zerboni, M. Signoretti, S. Crippa, M. Falconi, P.G. Arcidiacono, G. Capurso, Systematic review and meta-analysis: prevalence of incidentally detected pancreatic cystic lesions in asymptomatic individuals, Pancreatology 19 (1) (2019) 2–9.
[2] G.W. Charville, C.-S. Kao, Serous neoplasms of the pancreas: a comprehensive review, Arch. Pathol. Lab Med. 142 (9) (2018) 1134–1140.
[3] M.U. Tariq, Z. Ahmad, J. Abdul-Ghafar, N.U. Din, Serous cystadenoma of pancreas: a clinicopathologic experience of 23 cases from a major tertiary care center, Rare Tumors 10 (2018) 2036361318809183.
[4] L. Chu, A. Singhi, R. Haroun, R. Hruban, E. Fishman, The many faces of pancreatic serous cystadenoma: radiologic and pathologic correlation, Diagnostic and interventional imaging 98 (3) (2017) 191–202.
[5] K. Bramis, A. Petrou, A. Papalambros, et al., Serous cystadenocarcinoma of the pancreas: report of a case and management reflections, World J. Surg. Oncol. 10 (1) (2012) 1–5.
[6] A. McGuigan, P. Kelly, R.C. Turkington, C. Jones, H.G. Coleman, R.S. McCain, Pancreatic cancer: a review of clinical diagnosis, epidemiology, treatment and outcomes, World J. Gastroenterol. 24 (43) (2018) 4846.
[7] R. Wei, K. Lin, W. Yan, et al., Computer-aided diagnosis of pancreas serous cystic neoplasms: a radiomics method on preoperative MDCT images, Technol. Cancer Res. Treat. 18 (2019) 1533033818824339.
[8] M. D'Onofrio, E. Biagioli, C. Gerardi, et al., Diagnostic performance of contrast-enhanced ultrasound (CEUS) and contrast-enhanced endoscopic ultrasound (ECEUS) for the differentiation of pancreatic lesions: a systematic review and meta-analysis, Ultraschall in der Medizin-European Journal of Ultrasound 35 (6) (2014) 515–521.
[9] E.C. Amico, C.T.S. Salgado, L.M. Emerenciano, et al., Serous Cystadenoma of Pancreas: Why There Is Low Accuracy in Imaging Exams? ABCD Arquivos Brasileiros de Cirurgia Digestiva (São Paulo), 2022, p. 34.
[10] K. Ishigami, A. Nishie, Y. Asayama, et al., Imaging pitfalls of pancreatic serous cystic neoplasm and its potential mimickers, World J. Radiol. 6 (3) (2014) 36.
[11] S.R. Puli, N. Kalva, M.L. Bechtold, et al., Diagnostic accuracy of endoscopic ultrasound in pancreatic neuroendocrine tumors: a systematic review and meta analysis, World J. Gastroenterol.: WJG 19 (23) (2013) 3678.
[12] M. D'Onofrio, E. Barbi, C.F. Dietrich, et al., Pancreatic multicenter ultrasound study (PAMUS), Eur. J. Radiol. 81 (4) (2012) 630–638.
[13] M. D'Onofrio, S. Canestrini, R. De Robertis, et al., CEUS of the pancreas: still research or the standard of care, European journal of radiology 84 (9) (2015) 1644–1649.
[14] W. Liang, P. Yang, R. Huang, et al., A combined nomogram model to preoperatively predict histologic grade in pancreatic neuroendocrine tumors, Clin. Cancer Res. 25 (2) (2019) 584–594.
[15] P. Cejas, Y. Drier, K.M. Dreijerink, et al., Enhancer signatures stratify and predict outcomes of non-functional pancreatic neuroendocrine tumors, Nature medicine 25 (8) (2019) 1260–1265.
[16] M. Di Leo, L. Poliani, D. Rahal, et al., Pancreatic neuroendocrine tumours: the role of endoscopic ultrasound biopsy in diagnosis and grading based on the WHO 2017 classification, Dig. Dis. 37 (4) (2019) 325–333.
[17] G. Tedesco, A. Sarno, G. Rizzo, et al., Clinical use of contrast-enhanced ultrasound beyond the liver: a focus on renal, splenic, and pancreatic applications, Ultrasonography 38 (4) (2019) 278.
[18] V. Ciaravino, R. De Robertis, P. Tinazzi Martini, et al., Imaging presentation of pancreatic neuroendocrine neoplasms, Insights into imaging 9 (6) (2018) 943–953.
[19] M. Scialpi, A. Reginelli, A. D'Andrea, et al., Pancreatic tumors imaging: an update, Int. J. Surg. 28 (2016) S142–S155.
[20] R.F. Havre, S. Ødegaard, O.H. Gilja, L.B. Nesje, Characterization of solid focal pancreatic lesions using endoscopic ultrasonography with real-time elastography, Scand. J. Gastroenterol. 49 (6) (2014) 742–751.
[21] Y. Hirooka, T. Kuwahara, A. Irisawa, et al., JSUM ultrasound elastography practice guidelines: pancreas, J. Med. Ultrason. 42 (2) (2015) 151–174.
[22] C.F. Dietrich, M. Hocke, Elastography of the pancreas, current view, Clinical Endoscopy 52 (6) (2019) 533–540.
[23] X.-F. Tian, T.-T. Kuang, Y. Dong, et al., Prediction of pancreatic fistula after pancreatectomy by virtual touch tissue imaging and quantification (VTIQ) technology, Pancreatology 21 (8) (2021) 1498–1505.
[24] U. Vaish, T. Jain, A.C. Are, V. Dudeja, Cancer-associated fibroblasts in pancreatic ductal adenocarcinoma: an update on heterogeneity and therapeutic targeting, Int. J. Mol. Sci. 22 (24) (2021) 13408.
[25] T. Kuwahara, Y. Hirooka, H. Kawashima, et al., Quantitative evaluation of pancreatic tumor fibrosis using shear wave elastography, Pancreatology 16 (6) (2016) 1063–1068.
[26] P.S. Sidhu, V. Cantisani, C.F. Dietrich, et al., The EFSUMB guidelines and recommendations for the clinical practice of contrast-enhanced ultrasound (CEUS) in non-hepatic applications: update 2017 (long version), Ultraschall in der Medizin-European journal of ultrasound 39 (2) (2018) e2–e44.

[27] R. Zaro, M. Lupsor-Platon, A. Cheviet, R. Badea, The pursuit of normal reference values of pancreas stiffness by using Acoustic Radiation Force Impulse (ARFI) elastography, Medical Ultrasonography 18 (4) (2016) 425–430.
[28] R. Fluss, D. Faraggi, B. Reiser, Estimation of the Youden Index and its associated cutoff point, Biom. J.: Journal of Mathematical Methods in Biosciences 47 (4) (2005) 458–472.
[29] K.Y. Elbanna, H.-J. Jang, T.K. Kim, Imaging diagnosis and staging of pancreatic ductal adenocarcinoma: a comprehensive review, Insights into Imaging 11 (1) (2020) 1–13.
[30] C.F. Dietrich, C. Jenssen, Modern ultrasound imaging of pancreatic tumors, Ultrasonography 39 (2) (2020) 105.
[31] D. Gu, Y. Hu, H. Ding, et al., CT radiomics may predict the grade of pancreatic neuroendocrine tumors: a multicenter study, Eur. Radiol. 29 (12) (2019) 6880–6890.
[32] S.K. Jeon, J.M. Lee, I. Joo, et al., Nonhypervascular pancreatic neuroendocrine tumors: differential diagnosis from pancreatic ductal adenocarcinomas at MR imaging—retrospective cross-sectional study, Radiology 284 (1) (2017) 77–87.
[33] C-g Guo, S. Ren, X. Chen, et al., Pancreatic Neuroendocrine Tumor: Prediction of the Tumor Grade Using Magnetic Resonance Imaging Findings and Texture Analysis with 3-T Magnetic Resonance, Cancer management and research, 2019, pp. 1933–1944.
[34] X-q Zhang, R-q Zheng, J-y Jin, J-f Wang, T. Zhang, J. Zeng, US shear-wave elastography dispersion for characterization of chronic liver disease, Radiology 305 (3) (2022) 597–605.